Appl. Phys. A (2017) 123:766
DOI 10.1007/s00339-017-1392-5

Applied Physics A
Materials Science & Processing

Controlling the stainless steel surface wettability by nanosecond direct laser texturing at high fluences

P. Gregorčič[1] · B. Šetina-Batič[2] · M. Hočevar[2]

Received: 21 September 2017 / Accepted: 7 November 2017

Abstract This work investigates the influence of the direct laser texturing at high fluences (DLT-HF) on surface morphology, chemistry, and wettability. We use a Nd:YAG laser ($\lambda = 1064$ nm) with pulse duration of 95 ns to process stainless steel surface. The surface morphology and chemistry after the texturing is examined by using scanning electron microscopy (SEM), energy dispersive X-ray spectroscopy (EDS), and electron backscatter diffraction (EBSD), while the surface wettability is evaluated by measuring the static contact angle. Immediately after the texturing, the surface is superhydrophilic in a saturated Wenzel regime. However, this state is not stable and the superhydrophilic-to-superhydrophobic transition happens if the sample is kept in atmospheric air for 30 days. After this period, the laser-textured stainless steel surface expresses lotus-leaf-like behavior. By using a high-speed camera at 10,000 fps, we measured that the water droplet completely rebound from this superhydrophobic surface after the contact time of 12 ms.

1 Introduction

Surface is the outermost layer of any body. Therefore, its properties are of a great importance, since the interaction between the body and the environment takes place firstly on the body's surface. The importance of surface functionalities is easily recognized by the diversity of functional surfaces, developed in nature through the natural selection [1]. Here, one of the most known examples is a lotus leaf [2] with a hierarchical surface structure on micro (in the range of 10–20 μm) and nano (in the range of 100 nm to 2 μm) scale. This hierarchical structure results in superhydrophobicity (i.e., water super-repellency) and self-cleaning effect.

The inverse measure of the surface wettability is given by the contact angle θ, defined as the angle between the solid–liquid interface and the liquid–vapor interface. In the case of an ideal surface (i.e., flat, perfectly smooth, chemically homogenous, insoluble, non-reactive, and rigid [3]), the contact angle equals to the Young angle θ_Y obtained by the net force equation involving the surface tension between three phases: solid, liquid, and gas. If the Young angle is $\theta_Y < 90°$, the surface is defined as hydrophilic, if this angle exceeds 90°, the surface is hydrophobic, while superhydrophobic surface is defined as a surface, where the contact angle exceeds 150° [4].

When the roughness is added to an ideal surface, its wetting behavior is changed and can be described by two common states—by Wenzel [5] and Cassie–Baxter [6] state. In a Wenzel state, the liquid–solid interaction results in a *homogenous wetting*; in this case, the liquid is in a full contact with the (rough) solid surface, i.e., it completely penetrates in surface asperities, and the (Wenzel) contact angle θ_W is predicted by the following equation [5]:

$$\cos(\theta_W) = r\cos(\theta_Y). \quad (1)$$

Here, r stands for the roughness, defined as the ratio between the area of the rough surface and the area of the corresponding smooth surface. It is clearly seen from Eq. (1) that the roughness in Wenzel state always *gains* the wettability of the base material; consequently, it is impossible to obtain hydrophobic surface from hydrophilic material by adding the roughness, if the surface is in the Wenzel state.

✉ P. Gregorčič
peter.gregorcic@fs.uni-lj.si

[1] Faculty of Mechanical Engineering, University of Ljubljana, Aškerčeva 6, 1000 Ljubljana, Slovenia

[2] Institute of Metals and Technology, Lepi pot 11, 1000 Ljubljana, Slovenia

Published online: 13 November 2017

On contrary, this is possible in the Cassie–Baxter state, where *heterogeneous wetting* results as a consequence of a hierarchical surface structure. In this case, fraction f ($0 \leq f < 1$) of the solid surface area is in a contact with liquid, while another part ($1 - f$) of the solid surface is in the contact with gas. The Cassie–Baxter contact angle θ_{CB} is given by Eq. [6]:

$$\cos(\theta_{CB}) = f r_f \cos(\theta_Y) + f - 1, \quad (2)$$

where $r_f = r_f(f)$ is the roughness (defined equally as in the Wenzel state) of the wet area. In the limit case, when $f \rightarrow 1$, the surface wetting becomes homogeneous and the Cassie–Baxter equation [Eq. (2)] reduces to the Wenzel equation [Eq. (1)].

A significantly increased interest in the topic of controlled surface wettability is demonstrated in Fig. 1, which provides the number of citations per year to Wenzel [5] and Cassie and Baxter [6] papers in last 25 years (analyzed by using the ISI Web of Knowledge database). Currently, more than 1200 publications annually appear in the scientific literature. This significant scientific effort resulted in diversity of developed methods for the control of the surface wettability in laboratory environment [7–10]. One of these methods is also the direct laser texturing (DLT) that has been proven as an effective and flexible method for controlling the wettability on polydimethylsiloxane [11, 12], silicon [13], and metals [14–16].

By using the DLT, the surface wettability can be modified by one of the two main approaches. The first one is the *direct laser texturing with polarized pulses at (low) fluences* near the threshold fluence for laser ablation (*DLT-LF*). In this case, laser-induced periodic surface structures (LIPSS) appear on a surface as a regular ripple structure

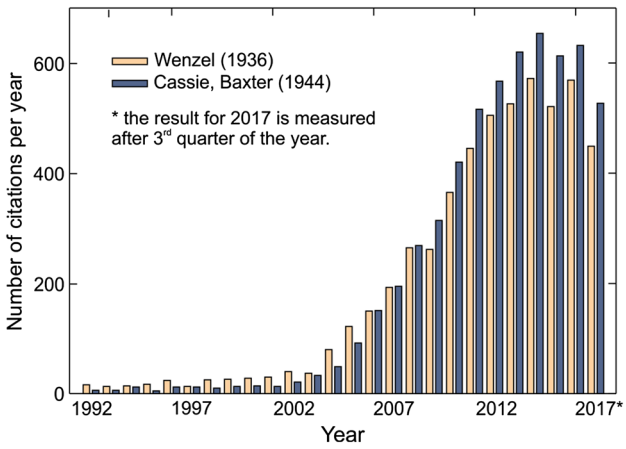

Fig. 1 Number of citations per year to the Wenzel [5] (the orange columns) and the Cassie and Baxter [6] (the blue columns) papers—matching on October 25th 2017 in the ISI Web of Knowledge database

with a period scaling well below to well above the laser wavelength, while its orientation and shape is defined by pulse polarization [17–20]. Here, periodic structure appears within a single laser spot and a large surface can be covered by overlapping laser pulses leading to coherent traces. The second approach is *direct laser texturing at high fluences (DLT-HF)*, where the pulse polarization is not so important. Here, the overlapping spots form micro(μ)-channels and a hierarchal structure appears due to material melting and oxidation [15, 16, 21–24].

The most of the work in the field of control of surface wettability by DLT has been done by DLT-LF approach, where ultrashort pulses (fs and ps) were usually used [13, 14, 17, 25–29]. However, in last two years, it has been successfully demonstrated that DLT-HF approach leads to similar results by reducing the complexity and the costs of the process [15, 16, 21–24]. Consequently, DLT-HF enables wider dissemination of this technology in diversity of industrial applications demanding simple, robust and costly acceptable method. Therefore, the main aim of this contribution is to show how direct laser texturing at high fluences influences on surface morphology and chemistry and, consequently, on its wettability.

2 Experimental

The surfaces of AISI 316L commercially available stainless steel were processed by direct laser texturing at high fluences. The as-received, non-polished samples were firstly ultrasonically cleaned in distilled water for 12 min and rinsed by ethanol. After the texturing, the modified surface morphology and chemistry were analyzed with different techniques, as described in subsection 2.2.

2.1 Direct laser texturing at high fluences

The stainless steel surfaces were placed in the focal plane of an F-theta lens (focal distance f_L = 160 mm). A scanner was used to lead the laser pulses (Nd:YAG laser, wavelength λ = 1064 nm) with pulse duration t_{FWHM} = 95 ns and pulse repetition rate f = 1 kHz in parallel lines, separated by Δy = 50 μm, over the surface. We used scanning velocity of v = 1.6 mm/s, while the beam spot size in focal position equaled 0.05 mm. Therefore, two adjacent pulses were separated by $\Delta x = v/f$ = 1.6 μm, which corresponds to high (97%) pulse overlapping. The average pulse power equaled 0.6 W resulting in a single pulse energy of 0.6 mJ and leading to peak fluence F_0 = 31 J cm^{-2}.

2.2 Surface characterization

After the laser texturing, the surfaces were kept in atmospheric air and were examined by the following methods:

(1) Scanning electron microscopy (SEM) was performed on DLT samples using JEOL JSM-6500F at 15 kV to evaluate the morphology modification after DLT-HF. SEM analysis was performed on top surface as well as on a cross section that was prepared by oxide polishing suspension (OPS) method.
(2) Energy dispersive X-ray spectroscopy (EDS; INCA Energy 400) was used to prove the appearance of an oxide layer after DLT-HF by measuring the weight percentage of the O element.
(3) The microstructural-crystallographic characteristics of the textured samples were examined by electron backscatter diffraction (EBSD) of the cross section (prepared by the OPS method).
(4) A static contact angle θ was measured at different times (0–30 days) after the DLT-HF by a goniometer of our own design. Here, a distilled-water droplet with a volume of 5 µL was delivered to the investigated surface. The image of the water droplet on the surface was captured by a CCD camera and the static contact angle was measured from the acquired image by fitting the line to the surface and by fitting the circle to the water droplet.
(5) A high-speed camera (FASTCAM SA-Z, Photron, USA) at 10,000 fps was used to measure the impact of a water droplet on (1) non-processed surface; (2) superhydrophilic surface (immediately after the laser texturing); and (3) superhydrophobic surface (30 days after the laser texturing).

3 Results and discussion

3.1 Influence of DLT-HF on surface morphology and chemistry

In the DLT-HF approach, the pulse fluences are significantly above the threshold fluence F_{th} for laser ablation. Therefore, the laser texturing in DLT-HF regime leads to µ-channels, while hierarchical structure appears due to melting and oxidation. In our case, we used $F_0 = 31$ J cm^{-2}. Due to high overlapping (97%) between the adjacent pulses, this leads to µ-channels, as clearly visible from SEM micrographs on Figs. 2 and 3.

The surface morphology after DLT-HF depends on peak fluence F_0 and scanning line separation Δy. The increased fluence results in deeper and wider µ-channels. In the case of a Gaussian beam, the µ-channel diameter D_μ in a focal position can be estimated from the fluence equation:

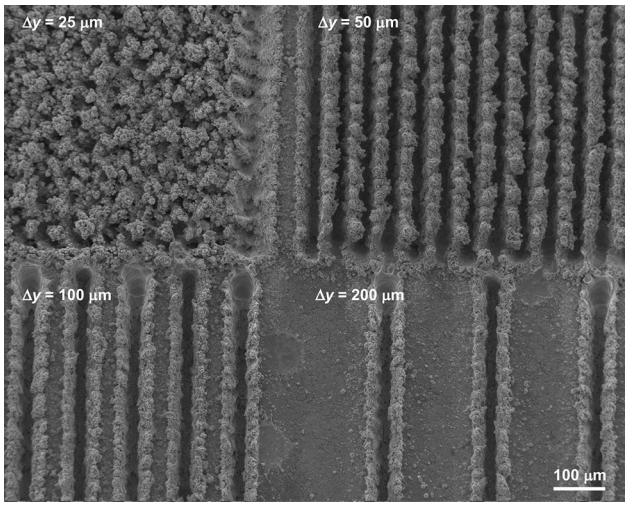

Fig. 2 SEM micrograph showing the influence of scanning line separation (Δy) on surface morphology at constant fluence $F_0 = 31$ J cm^{-2}

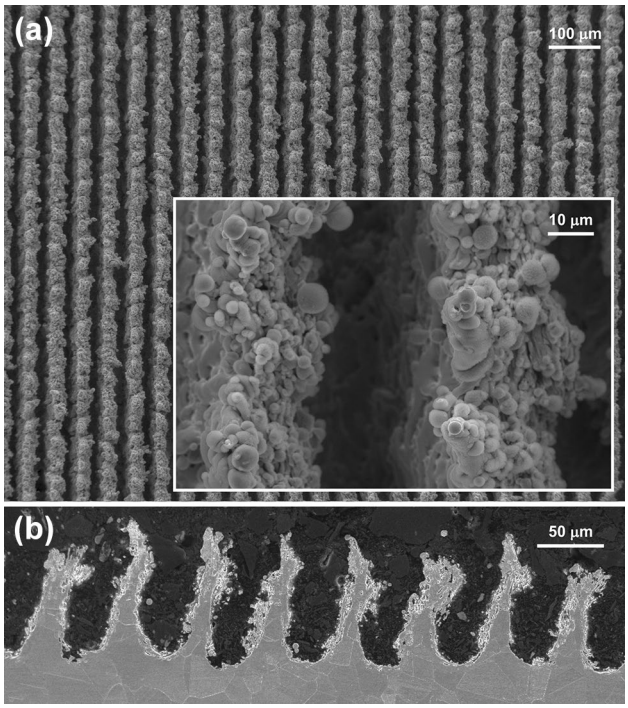

Fig. 3 **a** Surface morphology at two SEM magnifications after DLT-HF with $\Delta y = 50$ µm and $F_0 = 31$ J cm^{-2}. **b** SEM micrograph of the cross section

$$F_{th} = F_0 \exp\left(-\frac{D_\mu^2}{4w_0^2}\right), \quad (3)$$

where $w_0 = 25$ µm stands for the beam waist radius. By using Eq. (3), we estimate that the threshold fluence in our case equals $F_{th} = 7$ J cm^{-2}.

However, not only the fluence F_0, but also the scanning line reparation Δy significantly influences the surface morphology, as clearly revealed by SEM micrograph in Fig. 2 that shows the stainless-steel surface morphology for different Δy at a constant fluence $F_0 = 31$ J cm^{-2}. It is clearly visible that small scanning line separation (i.e., $\Delta y << D_\mu$) results in highly porous surface with no specific (long) µ-channels (see Fig. 2 for $\Delta y = 25$ µm). On contrary, as expected, large scanning line separation (i.e., $\Delta y >> D_\mu$) leads to well-separated µ-channels, as visible in Fig. 2 for $\Delta y = 200$ µm. As shown by Ta et al. [21, 22], scan line separation and surface roughness after DLT has also an influence on wettability. Within a short-term period (e.g., within 30 days) after laser texturing, smaller contact angle (higher wettability) is measured for smaller scan line separation [21] and for higher surface roughness [22].

To study the DLT-HF influence on surface wettability, we used the scanning line separation $\Delta y = 50$ µm that is just slightly smaller than D_μ; in our case, we estimate $D_\mu = 60$ µm. The surface morphology after laser texturing is presented in Fig. 3. A higher SEM magnification (the inset in Fig. 3) reveals that tips of µ-channels are covered with bumps having dimensions in the range of 1–7 µm. This bimodal surface morphology [16, 30] is also clearly visible from the cross section in Fig. 3b.

The laser texturing does not influence only the surface morphology, but also its chemistry [29, 30]. The oxide layer is clearly visible in Fig. 4a, where we made a SEM image of a bump with a broken oxide layer. The EDS measurements were performed in points 1–6 and within areas A (without the oxide layer) and B (covered by the oxide layer). The measured weight percentage of the O element within selected points and/or areas is shown in graph in Fig. 4b and proves that direct laser texturing results in surface oxidation.

To study the influence of the laser texturing on microstructural-crystallographic characteristics of the laser-textured material, we performed the EBSD analysis of the cross section. The results are presented in Fig. 5. The bulk, non-processed material (at the bottom) has austentic grains with typical dimensions between 20 and 30 µm and with some degree of twinning. It is clearly visible that both—bulk and processed (on tips)—materials have no specific orientation of grains. For our processing parameters, the influence of laser texturing is mainly limited to about 80 µm from the surface and has the most significant influence on the tips, where melting appears. After the laser ablation and melting, the tips still have crystalline structure, but with much finer grains with typical dimensions much below 10 µm.

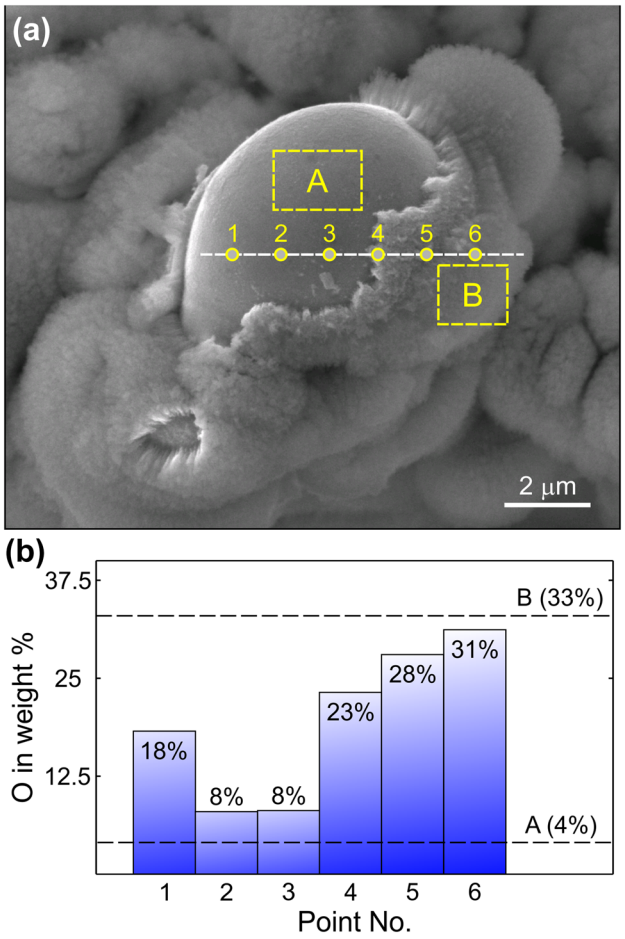

Fig. 4 **a** SEM micrograph of the part of surface (bump) with a broken oxide layer and **b** the analysis of the O element by using EDS

3.2 Surface wettability after DLT-HF

To evaluate the influence of the DLT-HF on the surface wettability, we measure the static contact angle at different times after the laser texturing. The surfaces were left on atmospheric air during this examination. For the reference, we measured also the wettability of the non-processed SS surface in the same time period.

As mentioned in "Experimental" section, we processed non-polished, as-received SS samples having the average roughness of a profile $R_a = 0.20 \pm 0.01$ µm. Direct laser texturing increases the roughness of the surface; in our case, roughness of the sample after DLT equaled $R_a = 16.1 \pm 0.28$ µm.

The contact angle on the controlling SS sample has not significantly changed over the time and equaled $\theta = 95.0° \pm 6.4°$. However, the contact angle of a base material (i.e., Young contact angle) can be measured only on an ideal flat surface [31–33]. Therefore, we highly polished ($R_a = 25 \pm 2$ nm) one of the non-processed SS

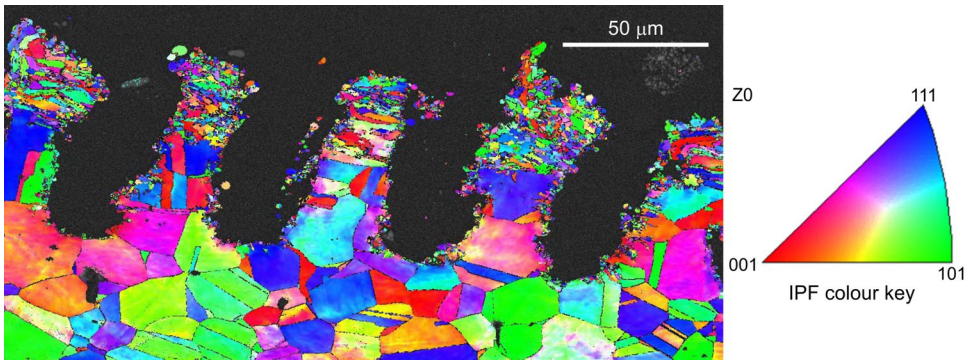

Fig. 5 EBSD measurement (*Z* direction IPF colouring orientation map) of the laser-textured surface

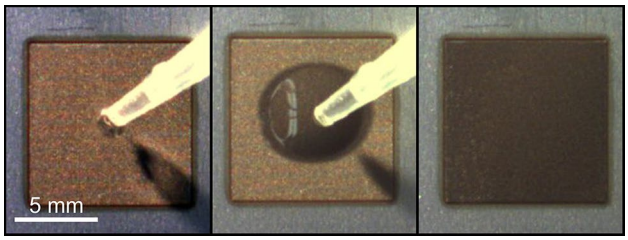

Fig. 6 Superhydrophilic surface in a saturated Wenzel regime immediately after the laser texturing

samples and measured the Young's contact angle to be $\theta_Y = 81.6° \pm 5.7°$.

Immediately after DLT-HF the water droplet spills over the whole sample and forms a thin film, as shown in Fig. 6. Therefore, the surface is superhydrophilic in a saturated Wenzel regime with contact angle $\theta = 0°$. The Wenzel state [Eq. (1)] predicts saturation of an ideal hydrophilic surface (with $\theta_Y < 90°$) to a film ($\theta_W = 0°$) when roughness r exceeds the saturated roughness r_S [34]:

$$r_S = \frac{1}{\cos(\theta_Y)} \tag{4}$$

In the case of our material, the saturated roughness equals $r_S = 6.8$. From cross section (Fig. 3b), we measured that the surface roughness after DLT-HF equals $r = 4.5 < r_S$. Saturated Wenzel state, therefore, additionally confirms that laser texturing changes also the surface chemistry (as was shown by EDS measurements on Fig. 4) and, consequently, its fundamental (Young) wettability. Since metal oxides are usually even more hydrophilic than metals, this explains the saturated Wenzel regime with roughness smaller than r_S calculated from the Young angle of the base (i.e., stainless steel) material; after the laser processing, the Young angle obviously decreases due to metal oxidation—this is additionally confirmed by the saturated Wenzel regime at roughness $r < r_S$. This results show that both, surface roughness and surface chemistry (appearance of the surface oxides), increase metallic surface wettability after DLT.

The superhydrophilic metal surface after laser texturing is not stable. If such a surface is left on the atmospheric air, the (super)hydrophobicity develops and the surface is transformed from the Wenzel state into the Cassie–Baxter state as has been previously shown by several authors [14–16, 22, 27]. In our case, the superhydrophobic surface with a static contact angle $\theta = 153°$ developed in 30 days, as shown in Fig. 7.

We should notice that the mechanisms responsible for transition from hydrophilic (Wenzel) to (super)hydrophobic (Cassie–Baxter) state after DLT is still under debate [16, 35]. Different authors proposed several (contradictory) theories trying to explain this transition. These theories propose mechanisms, such as decomposition of carbon dioxide

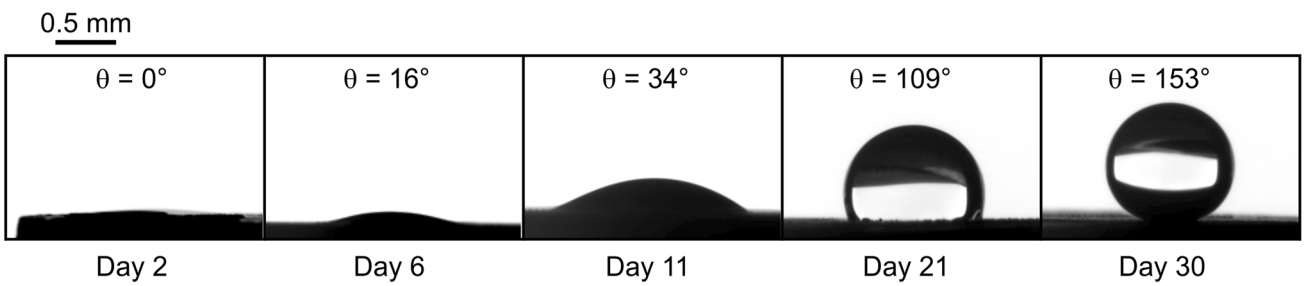

Fig. 7 Superhydrophobicity development after laser direct texturing

into carbon with active magnetite [14], airborne hydrocarbon contamination and the absorption of organic matters from the atmosphere [35, 36], partial surface deoxidation [37], and the creation of hydrophobic functional groups [26]. These several disputing theories indicate that further research is needed to answer this important and still opened question.

3.3 A bouncing droplet on a laser-textured surface

It has been shown that superhydrophobic surfaces reduce the contact time of a droplet rebound from them [38]. This is important, since the extent to which momentum, energy, and mass are exchanged between surface and droplet depends on the contact time. Therefore, we used a high-speed camera to measure the impact of a 5 μL droplet with (1) a non-processed stainless steel (Fig. 8); (2) the superhydrophilic surface (Fig. 9) immediately after the laser texturing ; and (3) the laser-textured stainless steel 30 days after the laser texturing (when became superhydrophobic with a static contact angle of $\theta = 153°$; Fig. 10). The droplet was dropped 15 mm above the tested surface and the impact velocity equaled ~ 0.5 mm s^{-1} for all three cases.

In the case of a water droplet impact on a non-processed SS sample, the droplet does not rebound from the surface, but is stays attached on it, as visible from Fig. 8. In a steady-state conditions, it reaches a static contact angle of $\theta = 95°$ (the steady-state conditions are not shown in Fig. 8, since they are achieved far later the capturing times). However, it is visible that within the first 30 ms, the droplet "tries" to rebound from the surface three times, but—due to strong adhesion forces—without any success. The first rebound starts, when the first collapse of the droplet ends; this happens around 4 ms after the impact. The comparison of the

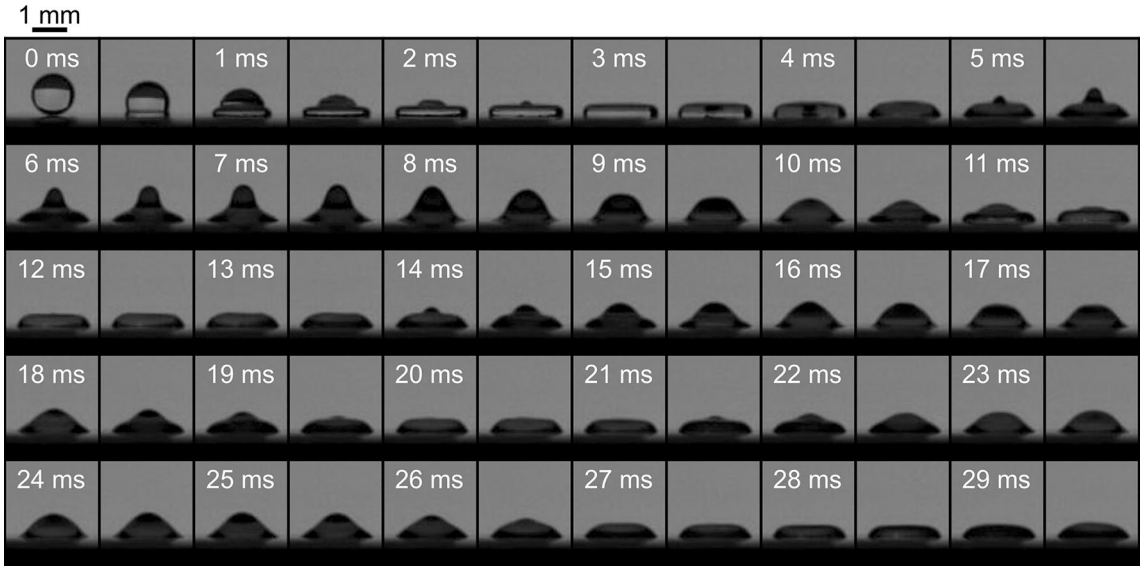

Fig. 8 Water drop bouncing on a surface of non-processed stainless steel ($\theta = 95°$). Each frame corresponds to time delay of 0.5 ms

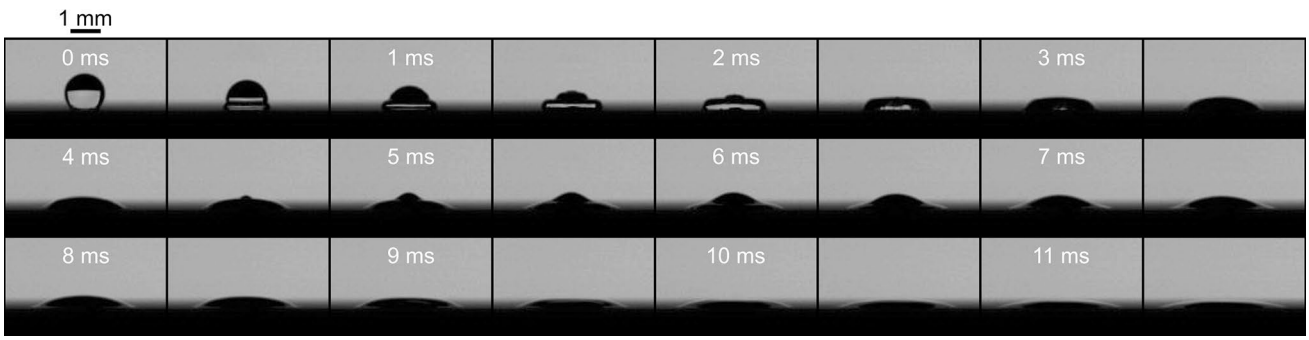

Fig. 9 Water drop bouncing on a superhydrophilic stainless-steel surface (immediately after laser texturing; $\theta = 0°$). Each frame corresponds to time delay of 0.5 ms

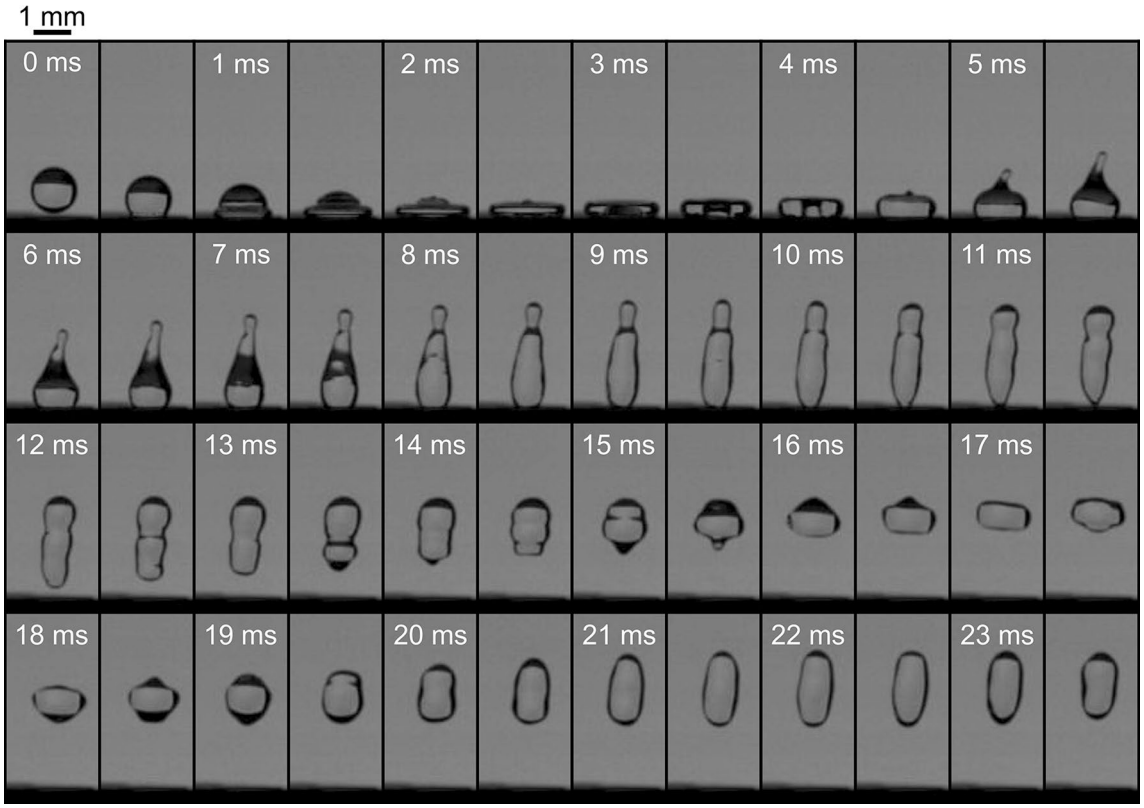

Fig. 10 Water drop bouncing on a superhydrophobic stainless-steel surface (left for 30 days after laser texturing in atmospheric air; $\theta = 153°$). Each frame corresponds to time delay of 0.5 ms

results in Figs. 8, 9, and 10 shows that this time does not significantly depend on the surface wettability.

Nevertheless, in the case of a superhydrophilic surface (Fig. 9), the stronger adhesion forces lead to higher attenuation of droplet vibrations and the droplet starts to form a water film approximately 8 ms after the impact.

The situation after the first droplet collapse (i.e., at times > 4 ms) is completely different in the case of the superhydrophobic surface. As visible from Fig. 10, the droplet completely rebounds from the surface 12 ms after its impact. The measured contact time of 12 ms is similar as a result obtained by Bird et al. [38] who used superhydrophobic surface, produced by laser ablation of silicon wafer coated with fluorosilane. This clearly confirms that nanosecond direct laser texturing at high fluences enables similar results as other methods for production of artificial superhydrophobic, lotus-leaf like surfaces.

4 Conclusions

We successfully used the direct laser texturing at high fluences by a nanosecond laser to produce the superhydrophobic, lotus-leaf-like stainless steel surface.

By using SEM analysis, we have shown that changing the scanning line separation can lead to completely different surface morphologies—from highly porous surface with not specifically visible μ-channels to well-separated μ-channels which width and depth depend on laser fluence. The EDS measurements confirm the appearance of the oxide film after the laser texturing. The change of the surface chemistry after DLT-HF is additionally confirmed by a surface in a saturated Wenzel state immediately after laser texturing resulting in a roughness lower than the saturated Wenzel roughness estimated from the Young angle of base material. On the other hand, the EBSD measurements reveal that the DLT-HF mainly influences the crystal grains on tips of μ-channels, where ablation and melting appear during laser–pulse–metal interaction. However, the molten material keeps crystalline structure, but with much finer grains—their dimensions reduce from 20 to 30 μm to less than 10 μm.

When the laser-textured surfaces are left on atmospheric air, the hydrophobicity starts to develop. In our case, the transition from superhydrophilic surface in a saturated Wenzel regime (appearing immediately after texturing) to superhydrophobic surface in a Cassie–Baxter regime with the contact angle of 153° happened in 30 days. The high-speed camera measurements of a droplet rebound on this

superhydrophobic stainless steel surface showed similar contact times as in the case of superhydrophobic surfaces, produced by other approaches. This confirms that the DLT-HF approach has the ability to achieve similar results as other methods, but with reduced complexity and costs of the process. This will open new possibilities for dissemination of this technology in a diversity of industrial applications.

Acknowledgements The authors acknowledge the financial support from the Slovenian Research Agency (research core funding Nos. P2-0392 and P2-0132).

References

1. F.A. Muller, C. Kunz, S. Graf, Materials **9**, 476 (2016)
2. W. Barthlott, C. Neinhuis, Planta **202**, 1 (1997)
3. T.S. Meiron, A. Marmur, I.S. Saguy, J. Colloid. Interf. Sci **274**, 637 (2004)
4. X.Y. Wang, D.M. Riffe, Y.-S. Lee, M.C. Downer, Phys. Rev. B **50**, 8016 (1994)
5. R.N. Wenzel, Ind. Eng. Chem **28**, 988 (1936)
6. A.B.D. Cassie, S. Baxter, T. Faraday Soc **40**, 0546 (1944)
7. T. Darmanin, E.T. de Givenchy, S. Amigoni, F. Guittard, Adv. Mater **25**, 1378 (2013)
8. S. Tawfick, M. De Volder, D. Copic, S.J. Park, C.R. Oliver, E.S. Polsen, M.J. Roberts, A.J. Hart, Adv. Mater., **24**, 1628 (2012)
9. D.Y. Xia, L.M. Johnson, G.P. Lopez, Adv. Mater **24**, 1287 (2012)
10. S.T. Wang, K.S. Liu, X. Yao, L. Jiang, Chem. Rev **115**, 8230 (2015)
11. M.T. Khorasani, H. Mirzadeh, P.G. Sammes, Radiat. Phys. Chem **47**, 881 (1996)
12. T.O. Yoon, H.J. Shin, S.C. Jeoung, Y.I. Park, Opt. Express **16**, 12715 (2008)
13. V. Zorba, L. Persano, D. Pisignano, A. Athanassiou, E. Stratakis, R. Cingolani, P. Tzanetakis, C. Fotakis, Nanotechnology **17**, 3234 (2006)
14. A.M. Kietzig, S.G. Hatzikiriakos, P. Englezos, Langmuir **25**, 4821 (2009)
15. D.V. Ta, A. Dunn, T.J. Wasley, R.W. Kay, J. Stringer, P.J. Smith, C. Connaughton, J.D. Shephard, Appl. Surf. Sci **357**, 248 (2015)
16. U. Trdan, M. Hočevar, P. Gregorčič, Corros. Sci **123**, 21 (2017)
17. A.Y. Vorobyev, C.L. Guo, Laser Photonics Rev **7**, 385 (2013)
18. J. Bonse, S. Hohm, S.V. Kirner, A. Rosenfeld, J. Kruger, IEEE J. Sel. Top. Quant **23**, 9000615 (2017)
19. J. Reif, C. Martens, S. Uhlig, M. Ratzke, O. Varlamova, S. Valette, S. Benayoun, Appl. Surf. Sci., **336**, (2015)
20. P. Gregorčič, M. Sedlaček, B. Podgornik, J. Reif, Appl. Surf. Sci **387**, 698 (2016)
21. V.D. Ta, A. Dunn, T.J. Wasley, J. Li, R.W. Kay, J. Stringer, P.J. Smith, E. Esenturk, C. Connaughton, J.D. Shephard, Appl. Surf. Sci **365**, 153 (2016)
22. V.D. Ta, A. Dunn, T.J. Wasley, J. Li, R.W. Kay, J. Stringer, P.J. Smith, E. Esenturk, C. Connaughton, J.D. Shephard, Appl. Surf. Sci **371**, 583 (2016)
23. M. Zupančič, M. Može, P. Gregorčič, I. Golobič, Appl. Surf. Sci **399**, 480 (2017)
24. D.M. Chun, C.V. Ngo, K.M. Lee, Cirp Ann-Manuf. Techn **65**, 519 (2016)
25. V. Zorba, E. Stratakis, M. Barberoglou, E. Spanakis, P. Tzanetakis, S.H. Anastasiadis, C. Fotakis, Adv. Mater **20**, 4049 (2008)
26. P. Bizi-bandoki, S. Valette, E. Audouard, S. Benayoun, Appl. Surf. Sci **273**, 399 (2013)
27. A.M. Kietzig, M.N. Mirvakili, S. Kamal, P. Englezos, S.G. Hatzikiriakos, J Adhes Sci Technol **25**, 2789 (2011)
28. M. Martinez-Calderon, A. Rodriguez, A. Dias-Ponte, M.C. Morant-Minana, M. Gomez-Aranzadi, S.M. Olaizola, Appl. Surf. Sci., **374** (2016)
29. S.V. Kirner, T. Wirth, H. Sturm, J. Krüger, J. Bonse, J. Appl. Phys., **122**, (2017)
30. L.B. Boinovich, A.M. Emelyanenko, A.D. Modestov, A.G. Domantovsky, K.A. Emelyanenko, Acs Appl. Mater. Inter **7**, 19500 (2015)
31. A. Marmur, Langmuir **19**, 8343 (2003)
32. A. Marmur, Soft Matter **2**, 12 (2006)
33. A. Sarkar, A.M. Kietzig, Chem. Phys. Lett. **574**, 106 (2013)
34. G. McHale, N.J. Shirtcliffe, M.I. Newton, Analyst **129**, 284 (2004)
35. L.B. Boinovich, A.M. Emelyanenko, K.A. Emelyanenko, A.G. Domantovsky, A.A. Shiryaev, Appl. Surf. Sci., **379** (2016)
36. J.Y. Long, M.L. Zhong, P.X. Fan, D.W. Gong, H.J. Zhang, J. Laser Appl., **27** (2015)
37. F.M. Chang, S.L. Cheng, S.J. Hong, Y.J. Sheng, H.K. Tsao, Appl. Phys. Lett., **96** (2010)
38. J.C. Bird, R. Dhiman, H.M. Kwon, K.K. Varanasi, Nature **503**, 385 (2013)